J. Fluid Mech. (1996), *vol.* 322, *pp.* 275–296

Ignition in the supersonic hydrogen/air mixing layer with reduced reaction mechanisms

By H. G. IM, B. T. HELENBROOK, S. R. LEE AND C. K. LAW

Department of Mechanical and Aerospace Engineering, Princeton University, Princeton, NJ 08544, USA

(Received 1 February 1994 and in revised form 22 March 1996)

Asymptotic analysis of ignition within the supersonic hydrogen/air mixing layer is performed using reduced mechanisms. Two distinct reduced mechanisms for the high-temperature and the low-temperature regimes are used depending on the characteristic temperature of the reaction zone relative to the crossover temperature at which the reaction rates of the $H + O_2$ branching and termination steps are equal. Each regime further requires two distinct analyses for the hot-stream and the viscous-heating cases, depending on the relative dominance of external and internal ignition energy sources. These four cases are analysed separately, and it is shown that the present analysis successfully describes the ignition process by exhibiting turning point or thermal runaway behaviour in the low-temperature regime, and radical branching followed by thermal runaway in the high-temperature regime. Results for the predicted ignition distances are then mapped out over the entire range of the parameters, showing consistent behaviour with the previous one-step model analysis. Furthermore, it is demonstrated that ignition in the low-temperature regime is controlled by a larger activation energy process, so that the ignition distance is more sensitive to its characteristic temperature than that in the high-temperature regime. The ignition distance is also found to vary non-monotonically with the system pressure in the manner of the well-known hydrogen/oxygen explosion limits, thereby further substantiating the importance of chemical chain mechanisms in this class of chemically reacting boundary layer flows.

1. Introduction

A major perceived difficulty in the development of scramjet technology is the extremely short residence time within the combustion chamber because of the associated high flow speed. Since flame holding in jet engines is mostly through ignition and combustion in the mixing layer (Marble & Adamson 1954), one of the fundamental phenomena of interest here is ignition in the laminar mixing layer. Understanding gained from such a simple configuration should provide insight into the more realistic, and complex situations involving turbulent mixing layers.

An interesting, and potentially important, recent theoretical result in the study of high-speed chemically reacting mixing layers is the recognition that ignition can actually be facilitated by increasing flow speed through the viscous conversion of the flow kinetic energy to thermal energy, which in turn increases the reaction rate. Specifically, the effect of viscous heating on ignition of supersonic mixing layers has been studied through an asymptotic approach (Jackson & Hussaini 1988; Grosch &

Jackson 1991) and by direct numerical calculation (Figueira da Silva *et al.* 1993). Asymptotic analysis in the ignition problem is particularly useful in that a proper dominant balancing readily yields an order-of-magnitude estimate for the minimum ignition distance, which is frequently represented by a relevant Damköhler number. Furthermore, by obtaining results in generalized reduced parameters, the ignition distance can be explicitly expressed in terms of the various system parameters.

In our recent studies (Im, Bechtold & Law 1993; Im *et al.* 1994) we have also performed numerical and asymptotic analyses of ignition within supersonic boundary layers, using a one-step overall reaction. As similarly recognized in the earlier study of Grosch & Jackson (1991), we have identified three distinct ignition regimes depending on the relative extents of viscous heating and the external heat source that elevates the hot boundary temperature. Results of the analysis can be interpreted by recognizing that $x_{ig} \sim u_\infty \exp(E_a/R^0 T_c)$, where x_{ig} is the ignition distance, u_∞ the free-stream velocity, E_a the activation energy, R^0 the gas constant and T_c the characteristic temperature of the ignition region. Therefore, starting from low speeds, the ignition distance initially increases linearly with the free-stream Mach number because T_c remains almost constant. However, as u_∞ further increases, T_c increases quadratically with the flow Mach number owing to viscous heating. Consequently, the ignition distance exponentially decreases. This therefore implies that ignition and flame stabilization in a supersonic boundary layer is a viable concept if the large kinetic energy of the flow can be utilized.

We now move one step forward and consider the effects of realistic chemistry associated with the hydrogen/air system in supersonic boundary layer ignition. This extension is meaningful for the following reasons. First, hydrogen is a strong candidate as a scramjet fuel because the limited residence time in the combustion chamber requires a fuel which has high energy density as well as high reactivity. Furthermore, hydrogen oxidation chemistry not only plays a fundamental role in hydrocarbon combustion, but its highly nonlinear chemical response to variations in temperature and pressure, due to the intrinsic kinetic coupling between the radicals and the reaction steps, provides a strong indication that the ignition phenomena can be significantly richer than those described by the simplified global one-step reaction. Some analyses have been recently performed on ignition in hydrogen/oxygen systems, including several analytical studies with reduced mechanisms. In particular, Treviño performed an asymptotic analysis of ignition for the homogeneous mixture (Treviño 1991) and for the flat-plate boundary layer flow of a premixed combustible (Treviño & Méndez 1991). Lee & Law (1994) analysed the ignition of a hydrogen flow by heated counterflowing air, using somewhat different reduced mechanisms. The study successfully reproduced the numerically observed (Kreutz & Law 1996) 'Z-curve' response to variations in the system pressure and temperature, which is analogous to the explosion limits of the homogeneous hydrogen/oxygen mixture.

The present work applies the reduced mechanisms of Lee & Law (1994) to ignition within the supersonic mixing layer. Specifically, two distinct reduced mechanisms have been identified depending on the maximum characteristic temperature of the ignition source, T_c, relative to the crossover temperature, T^*, at which the rates of the chain branching reaction $H + O_2 \rightarrow OH + O$ and the chain terminating reaction $H + O_2 + M \rightarrow HO_2 + M$ are equal. It is demonstrated that the ignition behaviour is properly captured by a two-step mechanism for the low-temperature regime and a three-step mechanism for the high-temperature regime. The ignition response for each of these two regimes further depends on whether the ignition source is mainly provided by the external hot stream or through internal viscous heating (Im *et al.* 1994). We

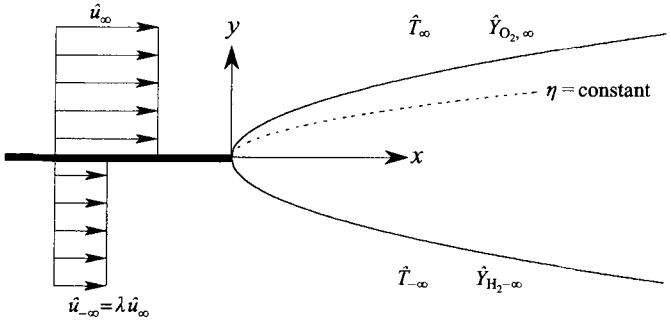

FIGURE 1. Schematic of the laminar mixing layer configuration.

shall therefore analyse these four different cases, and derive the ignition distance as a function of the various system parameters such as the free-stream velocity, free-stream temperature, and pressure. It will be shown in due course that the system response is indeed significantly enriched when realistic chemistry is properly taken into account.

2. Governing equations and boundary conditions

We consider a laminar mixing layer as shown in figure 1. Hydrogen is supplied in the lower stream with uniform velocity $\hat{u}_{-\infty}$, temperature $\hat{T}_{-\infty}$ and mass fraction $\hat{Y}_{H_2,-\infty}$, while air is supplied in the upper stream with $\hat{u}_\infty$, $\hat{T}_\infty$ and $\hat{Y}_{O_2,\infty}$. We employ the boundary layer approximation with zero pressure gradient such that the chemically frozen solution is self-similar. As the two reactants flow downstream and diffuse into one another, chemical reaction evolves and eventually leads to thermal runaway at a certain streamwise distance. We shall analyse the reaction zone structure up to the ignition point in order to predict the minimum distance to achieve ignition. For simplicity, we assume constant values of the specific heat and the Chapman–Rubesin parameter, $\hat{\rho}\hat{\mu}$, and unity Prandtl number as well as the Lewis numbers of species i, except those for H and H_2, for which $Le_H = 0.2$ and $Le_{H_2} = 0.3$ are used.

We introduce the similarity transverse coordinate

$$\eta = \eta_0 + \left(\frac{\hat{u}_\infty}{2\hat{\rho}_\infty\hat{\mu}_\infty x}\right)^{1/2}\int_0^y \hat{\rho}(x,\bar{y})\mathrm{d}\bar{y}, \tag{2.1}$$

where η_0 is the shift of the origin and x the streamwise coordinate. It is noted that η_0 may remain indeterminate (Klemp & Acrivos 1972), but we are free to translate the coordinate such that $\eta = 0$ along the trajectory of the original interface within the mixing layer. The conservation equations for momentum, static energy and species i in the supersonic mixing layer are then respectively expressed as (Im *et al.* 1994)

$$f''' + ff'' = 0, \tag{2.2}$$

$$\frac{\partial^2 T}{\partial\eta^2} + f\frac{\partial T}{\partial\eta} - 2xf'\frac{\partial T}{\partial x} = -\frac{2x}{\hat{u}_\infty\hat{\rho}}\frac{W_{H_2}}{\hat{Y}_{H_2,-\infty}}\sum_{m=1}^{M} q_m\omega_m - 2\mu\left[\frac{f''(\eta)}{1-\lambda}\right]^2, \tag{2.3}$$

$$\frac{1}{Le_i}\frac{\partial^2 Y_i}{\partial\eta^2} + f\frac{\partial Y_i}{\partial\eta} - 2xf'\frac{\partial Y_i}{\partial x} = -\frac{2x}{\hat{u}_\infty\hat{\rho}}\frac{W_{H_2}}{\hat{Y}_{H_2,-\infty}}\sum_{m=1}^{M}(\nu''_{i,m} - \nu'_{i,m})\omega_m, \tag{2.4}$$

which are supplemented by the ideal-gas equation of state. Here f is the stream

No.	Reaction	A	n	E_a
1f	$H + O_2 \rightarrow O + OH$	1.92×10^{14}	0.00	16440
2f	$O + H_2 \rightarrow H + OH$	5.08×10^{04}	2.67	6290
3f	$OH + H_2 \rightarrow H + H_2O$	2.16×10^{08}	1.51	3430
9f	$H + O_2 + M \rightarrow HO_2 + M$	6.17×10^{19}	−1.42	0
10b	$H_2 + O_2 \rightarrow HO_2 + H$	1.93×10^{14}	0.00	59610
14f	$HO_2 + HO_2 \rightarrow H_2O_2 + O_2$	3.02×10^{12}	0.00	1390
15f	$H_2O_2 + M \rightarrow OH + OH + M$	1.20×10^{17}	0.00	45500
17b	$H_2 + HO_2 \rightarrow H_2O_2 + H$	3.73×10^{13}	0.00	24110

TABLE 1. Rate coefficients of starting reaction mechanism for hydrogen in the form $k = AT^n \exp(-E_a/R^0T)$. Units are moles, cm^3, seconds, Kelvin and calories/mole.

function $\psi(x, y)$ normalized as $f(\eta) = \psi(x, y)/(2\hat{\rho}_\infty \hat{\mu}_\infty \hat{u}_\infty x)^{1/2}$. Furthermore, the non-dimensional temperature, T, and the mass fraction for species i, Y_i, are defined in terms of their physical counterparts $\hat{T}$ and $\hat{Y}_i$ as $T = c_p \hat{T} W_{H_2}/Q\hat{Y}_{H_2,-\infty}$ and $Y_i = \hat{Y}_i W_{H_2}/\hat{Y}_{H_2,-\infty} W_i$, where $Q = \sum_i \sum_m h_i^0 W_i (v''_{i,m} - v'_{i,m})$ is the total heat release, $q_m = -\sum_i h_i^0 W_i (v''_{i,m} - v'_{i,m})/Q$ the fractional heat release of each reaction step with respect to Q, and the indices i and m respectively denote the species and the reaction steps. The last term in (2.3) represents the heat generated by viscous heating, indicated by the parameter $\mu \equiv (1/2)(\gamma - 1)M_\infty^2 T_\infty (1 - \lambda)^2$, where $\gamma = c_p/c_v$, $\lambda = \hat{u}_{-\infty}/\hat{u}_\infty$, and $M_\infty = \hat{u}_\infty/(\gamma R^0 \hat{T}_\infty/\bar{W})^{1/2}$ is the Mach number of the upper faster air free-stream.

Equations (2.2)–(2.4) are subject to the boundary conditions

$$\left.\begin{aligned} f' = 1, \quad T = T_\infty, \quad Y_{O_2} = Y_{O_2,\infty}, \quad Y_{i \neq O_2} = 0; \quad \eta \rightarrow \infty, \\ f' = \lambda, \quad T = T_\infty - \beta, \quad Y_{H_2} = 1, \quad Y_{i \neq H_2} = 0; \quad \eta \rightarrow -\infty, \\ f(0) = 0, \end{aligned}\right\} \tag{2.5}$$

where $\beta = T_\infty - T_{-\infty}$. In this study we only consider the case of $\beta > 0$ and $O(1)$, such that the air stream is considerably hotter than the hydrogen stream. Throughout the presentation of results we use $\hat{Y}_{H_2,-\infty} = 1$, $\hat{Y}_{O_2,\infty} = 0.233$, $\lambda = 0.5$, and $\hat{T}_{-\infty} = 500\,\text{K}$.

It is noted that the present study is only concerned with events up to the ignition point and therefore we have employed the parabolic system of equations (2.2)–(2.4). Once ignition starts, the abrupt rise in temperature and radical concentration generates a large streamwise diffusion, and consequently a fully elliptic system may have to be considered for a more accurate description of such behaviour. We further remark that the momentum equation (2.2) with its boundary conditions is decoupled from the energy and species equations and can be solved independently to yield the self-similar Blasius profile for mixing layer flows (Lock 1951).

To simplify the chemical reaction terms, we adopt the reduced mechanisms of the hydrogen/oxygen system that have been derived by Lee & Law (1994) from a short mechanism consisting of eight elementary steps (Treviño & Méndez 1991), which are listed in table 1.

We shall analyse in the following two sections ignition in the low-temperature and high-temperature regimes, which respectively represent situations in which the charactersitic temperature of the ignition region is lower and higher than the crossover temperature T^*. For each of these regimes, we shall further study the hot-stream case and the viscous-heating case, depending on whether ignition is dominated by the external energy source or the internal source, which are respectively represented

by the parameter β and μ identified above. To reduce the extent of presentation, the 'intermediate case' in which the two ignition sources are comparable in magnitude is not considered in this paper. The analysis can be conducted by combining the present and previous (Im *et al.* 1993, 1994) approaches.

3. The low temperature regime

When the characteristic temperature of the ignition zone is lower than the crossover temperature, T^*, using the steady-state approximation for all radicals except H_2O_2, a two-step reduced mechanism has been derived as (Lee & Law 1994)

$$3H_2 + 2O_2 \rightarrow 2H_2O + H_2O_2, \tag{I}$$

$$2H_2 + O_2 \rightarrow 2H_2O, \tag{II}$$

whose reaction rates are expressed as $\omega_I = \omega_{1f} + \omega_{10b} + \omega_{17b}$ and $\omega_{II} = -\omega_{10b} + \omega_{15f} - \omega_{17b} \approx \omega_{15f}$, since $\omega_{15f} \gg \omega_{10b}, \omega_{17b}$. Although not apparent from the above expressions, step I can be interpreted as that of radical generation primarily through the elementary steps $1f$ and $17b$, while step II is the dominant heat release step through H_2O_2 branching ($15f$). Reaction $10b$ in step I represents radical initiation, which is relatively slow but has to be retained in an evolutionary system, as will be shown later. Furthermore, step I is almost thermally neutral and thus its contribution in the energy equation is neglected. The steady-state approximation also yields the concentrations of the steady-state species in algebraic forms as

$$[HO_2] = \{\hat{k}_{15f}[H_2O_2][M]/\hat{k}_{14f}\}^{1/2}, \tag{3.6}$$

$$[H] = \frac{2\hat{k}_{15f}[H_2O_2][M] + \hat{k}_{17b}[H_2]\{\hat{k}_{15f}[H_2O_2][M]/\hat{k}_{14f}\}^{1/2}}{\hat{k}_{1f}[O_2](\kappa - 2)}, \tag{3.7}$$

where $\kappa = \omega_{9f}/\omega_{1f} = \hat{k}_{9f}[M]/\hat{k}_{1f}$, such that $\kappa = 2$ when the temperature takes the crossover value. It is noted that the concentration of H blows up as $\kappa \rightarrow 2$, which implies that the steady-state condition, (3.7), is no longer valid as the temperature approaches the crossover value. An analysis of the behaviour near the crossover temperature may be conducted by rescaling variables with $(\kappa - 2)$ as a small parameter. Although this has not been performed in the present study, it is expected that such an analysis can provide a smooth transition from the low-temperature to the high-temperature regime.

Since the momentum equation (2.2) is not affected by other equations, $f(\eta)$ is a known function for given λ. Therefore, we only need to solve the equations for temperature and $[H_2O_2]$. It is convenient to use the convection-free coordinate

$$\xi = \int_{\eta}^{\infty} f'' \mathrm{d}\bar{\eta} \Big/ \int_{-\infty}^{\infty} f'' \mathrm{d}\bar{\eta} = (1 - f')/(1 - \lambda), \tag{3.8}$$

and the normalized streamwise coordinate

$$\zeta_\ell = x \left(\frac{4\hat{\rho}}{\hat{u}_\infty \bar{W}} \right) A_{15f} \mathrm{e}^{-T_{a,15f}/T_i}, \tag{3.9}$$

where the subscript ℓ denotes the low-temperature regime and $T_{a,m} = c_p E_{a,m}/R^0 \hat{Y}_{H_2,-\infty}$ is the non-dimensional activation temperature of reaction m. Using the algebraic

expressions (3.6) and (3.7) for [H] and [HO_2], we derive the conservation equations

$$\left[\frac{f''(\eta)}{1-\lambda}\right]^2 \frac{\partial^2 T}{\partial \xi^2} - 2\zeta_\ell[1-(1-\lambda)\xi]\frac{\partial T}{\partial \zeta_\ell} = -\zeta_\ell k_{15f} Y_{H_2O_2} - 2\mu\left[\frac{f''(\eta)}{1-\lambda}\right]^2, \tag{3.10}$$

$$\begin{aligned}\left[\frac{f''(\eta)}{1-\lambda}\right]^2 \frac{\partial^2 Y_{H_2O_2}}{\partial \xi^2} - 2\zeta_\ell[1-(1-\lambda)\xi]\frac{\partial Y_{H_2O_2}}{\partial \zeta_\ell} \\ = -\zeta_\ell\left[k_{15f}\left(\frac{Y_{H_2O_2}}{\kappa-2} + \Gamma_1 Y_{H_2} Y_{H_2O_2}^{1/2}\right) + \Gamma_2 k_{10b} Y_{H_2} Y_{O_2}\right],\end{aligned} \tag{3.11}$$

where

$$\Gamma_1 = \frac{1}{2}\left(1+\frac{1}{\kappa-2}\right)\left(\frac{\bar{W}\hat{Y}_{H_2,-\infty}}{W_{H_2}}\right)^{1/2}\frac{k_{17b}}{(k_{14f}k_{15f})^{1/2}}, \tag{3.12}$$

$$\Gamma_2 = \frac{1}{2}\left(\frac{\bar{W}\hat{Y}_{H_2,-\infty}}{W_{H_2}}\right), \tag{3.13}$$

and $k_m = \hat{k}_m(T)/\hat{k}_{15f}(T_c)$ is the rate constant of reaction m normalized by that of reaction 15f evaluated at T_c. Boundary conditions are the same as (2.5) except now $\xi = 0$ and $\xi = 1$ respectively denote the oxidizer and the hydrogen streams.

In summary, we recognize from (3.10) and (3.11) that ignition in the low-temperature regime is characterized by the production of H_2O_2 radicals (step I), followed by heat release through the branching of H_2O_2 radicals (step II). Therefore, the reaction source term in the energy equation (3.10) is represented by the rate of step II, while the three source terms in the conservation equation for H_2O_2, (3.11), respectively denote the production of H_2O_2 through the elementary steps $1f$, $17b$ and $10b$. It is noted that the direct effect of step $1f$ disappears owing to the use of the algebraic expressions (3.6) and (3.7) through the steady-state approximation.

In the limit of vanishing reactivity, we obtain the self-similar frozen temperature expressed as

$$T_f = T_\infty - \alpha\xi - \mu\xi^2, \tag{3.14}$$

where $\alpha = \beta - \mu$. As discussed in previous studies (Im *et al.* 1993, 1994), ignition in the hot-stream case ($\alpha > 0$) is governed by external heating and thus reaction occurs near the hot boundary, $\xi = 0$, while in the viscous-heating case ($\alpha < 0$) the ignition point occurs within the mixing layer, at $\xi_c = (1-\beta/\mu)/2$. We now proceed with the analysis for these two situations.

3.1. *The hot-stream case:* $\alpha > 0$

In this case, the maximum temperature in the mixing layer, T_c, is equal to T_∞, and reaction is confined to a layer of $O(\epsilon_\ell)$ thickness near the hot oxidizer stream, where $\epsilon_\ell \equiv T_c^2/T_{a,15f}$ is the small parameter of expansion. Introducing a stretched coordinate $\chi_\ell = \alpha\xi/\epsilon_\ell$, perturbing the temperature and the mass fraction of H_2O_2 inside the reaction zone as

$$T_{in} = T_f(\chi_\ell) + \epsilon_\ell\theta(\chi_\ell, \zeta_\ell) + O(\epsilon_\ell^2), \tag{3.15}$$

$$Y_{H_2O_2,in} = \epsilon_\ell(\kappa_\infty - 2)^{-1}\phi(\chi_\ell, \zeta_\ell) + O(\epsilon_\ell^2), \tag{3.16}$$

and using the asymptotic relations (Im *et al.* 1994; Lee & Law 1994)

$$Y_{H_2,in} = y_{H_2}^0 \xi^{Le_{H_2}} + O(\epsilon_\ell), \tag{3.17}$$

$$[f''/(1-\lambda)]^2 \sim -\xi^2 \ln \xi^2 \quad \text{as} \quad \xi \to 0, \tag{3.18}$$

where

$$y^0_{H_2} = \frac{(-2\ln \epsilon_\ell)^{(Le_{H_2}-1)/2}}{Le_{H_2}(1-\lambda)^{Le_{H_2}} \int_{-\infty}^{\infty} (f'')^{Le_{H_2}} \, d\eta}, \tag{3.19}$$

the inner structure equations are derived in locally similar forms as

$$\chi_\ell^2 \frac{\partial^2 \theta}{\partial \chi_\ell^2} = -\Delta \phi \exp(\theta - \chi_\ell), \tag{3.20}$$

$$\chi_\ell^2 \frac{\partial^2 \phi}{\partial \chi_\ell^2} = -\Delta(\phi + \bar{\Gamma}_1 \chi_\ell^{Le_{H_2}} \phi^{1/2}) \exp(\theta - \chi_\ell), \tag{3.21}$$

where

$$\Delta = \frac{\zeta_\ell}{(\kappa_\infty - 2)\ln \epsilon_\ell^{-2}}, \tag{3.22}$$

$$\bar{\Gamma}_1 = \Gamma_1 \frac{(\kappa_\infty - 2)^{3/2}}{\epsilon_\ell^{1/2}} y^0_{H_2}, \tag{3.23}$$

and the subscript ∞ denotes evaluation at the hot-stream boundary. The boundary conditions for the above structure equations (3.20) and (3.21) are obtained by matching with the outer solutions, given by

$$\theta(0) = \phi(0) = 0, \quad (\partial\theta/\partial\chi_\ell)(\infty) = (\partial\phi/\partial\chi_\ell)(\infty) = 0. \tag{3.24}$$

We remark that in deriving the structure equation for H_2O_2, the contribution of the last term on the right-hand side of the original species equation (3.11), which represents the chain initiation step, is very small and is thus neglected in this locally similar structure problem.

The system of equations (3.20), (3.21) and (3.24) has been solved numerically, using a second-order finite difference scheme and quasi-linearization of the nonlinear reaction terms. Given the boundary conditions (3.24), the solutions for θ and ϕ increase monotonically with χ_ℓ and asymptotically approach constant values as $\chi_\ell \to \infty$. Figure 2 shows the typical behaviour of the maximum values of the solutions $\theta(\infty)$ and $\phi(\infty)$ as functions of the reduced Damköhler number Δ, for $\bar{\Gamma}_1$ calculated at conditions of 1 atm and $\hat{T}_\infty = 900\,\text{K}$. It is clearly seen that the perturbations in temperature and radical concentration increase with Δ, and eventually exhibit the turning point behaviour. This turning point is defined as the ignition state for the present case. As the Damköhler number is increased beyond this point, a rapid transition to an ignited state occurs. We remark that, owing to the stiffness of equations (3.20) and (3.21) near $\chi_\ell = 0$, the numerical solutions for θ and ϕ are somewhat sensitive to the changes in the grid size. Nevertheless, the error in the ignition turning point, Δ_{ig}, still remains within a few percent and we have obtained a reasonable accuracy for the grid size of 10^{-3}, which has been used in the present calculation. Since there is only one parameter, $\bar{\Gamma}_1$, in the system, extensive solutions have been obtained and subsequently correlated as a function of $\bar{\Gamma}_1$ for Δ at ignition, given by

$$\Delta_{ig} = 0.26 \bar{\Gamma}_1^{-0.64}, \tag{3.25}$$

which is valid for $Le_{H_2} = 0.3$. With Δ_{ig} known, using (3.22) and (3.9) we can determine the ignition distance in terms of the streamwise coordinate.

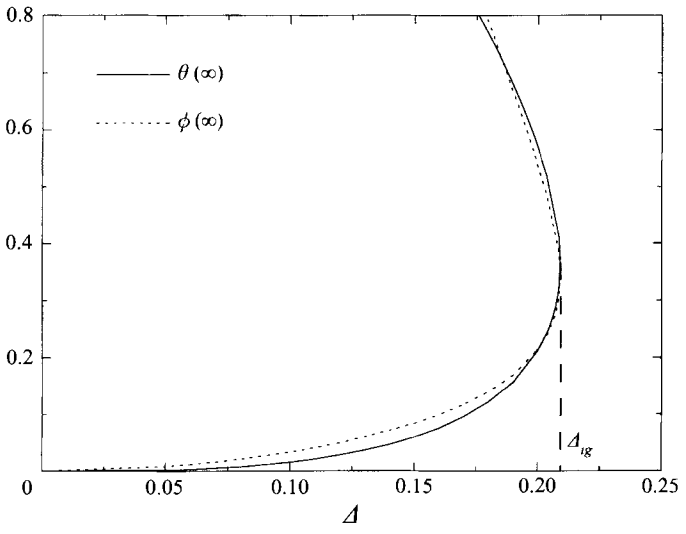

FIGURE 2. Typical behaviour of the solutions to equations (3.20), (3.21) and (3.24) for $\hat{T}_\infty = 900$ K, $\hat{u}_\infty = 600$ m s^{-1}, and $p = 1$ atm: the maximum values of the perturbed solutions as a function of the reduced Damköhler number.

3.2. *The viscous heating case:* $\alpha < 0$

As viscous heating overrides external heating, the maximum frozen temperature, $T_c = T_\infty + \alpha^2/4\mu$, occurs in the interior of the mixing layer, at $\xi_c = -\alpha/2\mu$. The frozen temperature profile then becomes parabolic, which suggests a broader stretched coordinate as $Z_\ell = \mu^{1/2}(\xi - \xi_c)/\epsilon_\ell^{1/2}$. The reduced Damköhler number appearing in the structure equation now has to be re-scaled by $O(\epsilon_\ell^{1/2})$, since otherwise only the trivial solution is obtained. Furthermore, unlike the hot-stream case, the term involving $Y_{H_2O_2}^{1/2}$ in (3.11) now becomes larger as Y_{H_2} in the reaction zone becomes $O(1)$. In such a case, owing to the different reaction orders of the key reaction rates in the energy and species equations, perturbations in temperature and the mass fraction of H_2O_2 cannot be similarly scaled. Therefore, a different scaling, other than ϵ_ℓ, is required for the perturbation of the radical concentration in order to capture the runaway phenomenon. Consequently, we perturb the solutions in the reaction zone as

$$T_{in} = T_f(Z_\ell) + \epsilon_\ell \tilde{\theta}_0(Z_\ell, \zeta_\ell) + \epsilon_\ell^{3/2}\tilde{\theta}_1(Z_\ell, \zeta_\ell) + O(\epsilon_\ell^2), \tag{3.26}$$

$$Y_{H_2O_2,in} = \delta(\kappa_c - 2)^{-1}[\tilde{\phi}_0(Z_\ell, \zeta_\ell) + \epsilon_\ell^{1/2}\tilde{\phi}_1(Z_\ell, \zeta_\ell)] + O(\delta\epsilon_\ell^{1/2}), \tag{3.27}$$

and seek the relation between ϵ_ℓ and δ. The appropriate distinguished limit turns out to be $\delta = \epsilon_\ell^{2/3}$, which physically implies that the increase of the radical concentration is faster than the temperature perturbation in terms of the present normalized quantities. Hence (3.27) is rewritten as

$$Y_{H_2O_2,in} = \epsilon_\ell^{2/3}(\kappa_c - 2)^{-1}[\tilde{\phi}_0(Z_\ell, \zeta_\ell) + \epsilon_\ell^{1/2}\tilde{\phi}_1(Z_\ell, \zeta_\ell)] + O(\epsilon_\ell^{5/3}). \tag{3.28}$$

Substituting (3.26) and (3.28) into the governing equations (3.10) and (3.11), and re-scaling the reduced Damköhler numbers, the structure equations at the first two orders become

$$\frac{\partial^2\tilde{\theta}_0}{\partial Z_\ell^2} = 0, \qquad \frac{\partial^2\tilde{\phi}_0}{\partial Z_\ell^2} = 0, \tag{3.29}$$

$$\left.\begin{aligned}\frac{\partial^2\tilde{\theta}_1}{\partial Z_\ell^2} &= -\tilde{\Delta}\tilde{\phi}_0\exp(\tilde{\theta}_0 - Z_\ell^2),\\ \frac{\partial^2\tilde{\phi}_1}{\partial Z_\ell^2} &= -\tilde{\Delta}\{\tilde{\Gamma}_1\tilde{\phi}_0^{1/2}\exp(\tilde{\theta}_0 - Z_\ell^2) + \tilde{\Gamma}_2\exp[\gamma_\ell(\tilde{\theta}_0 - Z_\ell^2)]\},\end{aligned}\right\} \tag{3.30}$$

where

$$\tilde{\Delta} = \frac{\epsilon_\ell^{1/6}\zeta_\ell}{\mu[f_c''/(1-\lambda)]^2(\kappa_c - 2)}, \tag{3.31}$$

$$\tilde{\Gamma}_1 = \Gamma_1(\kappa_c - 2)^{3/2}Y_{H_2,c}, \tag{3.32}$$

$$\tilde{\Gamma}_2 = \epsilon_\ell^{1/3}\Gamma_2(\kappa_c - 2)^2 k_{10b,c}Y_{H_2,c}Y_{O_2,c}, \tag{3.33}$$

$\gamma_\ell = T_{a,10b}/T_{a,15f}$, and the subscript c denotes evaluation at the location of the maximum temperature. Integration of the above equations (3.29)–(3.30) then provides the jump conditions across the reaction sheet for the outer solutions, which is to be solved next.

Temperature and the mass fraction of H_2O_2 for the outer zone are expanded as

$$T_{out} = T_f(\xi) + \epsilon_\ell\Theta_0(\xi,\tau_\ell) + O(\epsilon_\ell^{3/2}), \tag{3.34}$$

$$Y_{H_2O_2,out} = \epsilon_\ell^{2/3}(\kappa_c - 2)^{-1}\Phi_0(\xi,\tau_\ell) + O(\epsilon_\ell^{7/6}). \tag{3.35}$$

Substituting the above expansions into (3.10) and (3.11), and introducing the streamwise coordinate $\tau_\ell = \ln((\pi\mu)^{1/2}\tilde{\Delta})$, the leading-order equations for the temperature and species perturbations can be derived as

$$\frac{\partial^2\Theta_0}{\partial\xi^2} - \frac{2[1-(1-\lambda)\xi]}{[f''/(1-\lambda)]^2}\frac{\partial\Theta_0}{\partial\tau_\ell} = 0, \quad \xi \neq \xi_c, \tag{3.36}$$

$$\frac{\partial^2\Phi_0}{\partial\xi^2} - \frac{2[1-(1-\lambda)\xi]}{[f''/(1-\lambda)]^2}\frac{\partial\Phi_0}{\partial\tau_\ell} = 0, \quad \xi \neq \xi_c, \tag{3.37}$$

subject to the boundary and initial conditions

$$\left.\begin{aligned}&\Theta_0(0,\tau_\ell) = \Theta_0(1,\tau_\ell) = \Theta_0(\xi,-\infty) = 0,\\ &\Phi_0(0,\tau_\ell) = \Phi_0(1,\tau_\ell) = \Phi_0(\xi,-\infty) = 0.\end{aligned}\right\} \tag{3.38}$$

Matching with the inner solution yields the jump relations across the reaction zone as

$$\left.\begin{aligned}\left[\frac{\partial\Theta_0}{\partial\xi}\right]_{\xi_c^-}^{\xi_c^+} &= \frac{\partial\Theta_0}{\partial\xi}(\xi_c^+,\tau_\ell) - \frac{\partial\Theta_0}{\partial\xi}(\xi_c^-,\tau_\ell) = -\Phi_0(\xi_c,\tau_\ell)\exp[\Theta_0(\xi_c,\tau_\ell) + \tau_\ell],\\ \left[\frac{\partial\Phi_0}{\partial\xi}\right]_{\xi_c^-}^{\xi_c^+} &= -\tilde{\Gamma}_1\Phi_0^{1/2}(\xi_c,\tau_\ell)\exp[\Theta_0(\xi_c,\tau_\ell) + \tau_\ell] - \frac{\tilde{\Gamma}_2}{\gamma_\ell^{1/2}}\exp[\gamma_\ell\Theta_0(\xi_c,\tau_\ell) + \tau_\ell].\end{aligned}\right\} \tag{3.39}$$

We remark that, unlike the hot-stream case, the chain initiation term, $\omega_{10,b}$ on the right-hand side of the equation for H_2O_2, is retained even though it is very small. This is needed because the present equations are evolutionary such that some initiation is needed in order to trigger the reaction sequence. Otherwise only the trivial solution is obtained.

The system (3.36)–(3.39) is solved numerically using a second-order implicit finite difference scheme with a Newton iteration to handle the nonlinear reaction terms, and

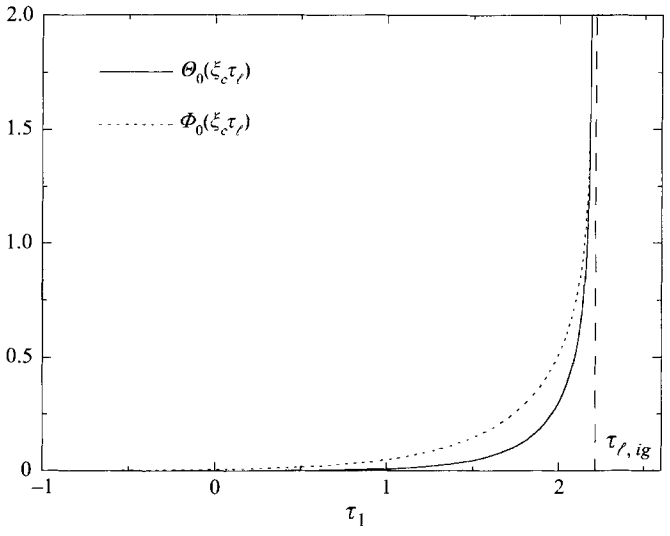

FIGURE 3. Typical behaviour of the solution to equations (3.36)–(3.39) for $\hat{T}_\infty = 800$ K, $\hat{u}_\infty = 3000$ m s^{-1}, and $p = 1$ atm: the maximum values of the perturbed solutions as a function of the non-dimensional streamwise coordinate.

where the streamwise step size is readjusted as the solution approaches the ignition point in order to capture the abrupt rise in the solutions. We have used sufficiently small grid sizes for both transverse and streamwise directions in order to ensure accurate results.

The profiles of Θ_0 and Φ_0 for a given value of τ_ℓ possess sharp peaks at $\xi = \xi_c$, and figure 3 shows those peak values along the τ_ℓ-direction, where $\tilde{T}_1$ and $\tilde{T}_2$ were calculated at conditions of 1 atm, $\hat{T}_\infty = 800$ K, and $\hat{u}_\infty = 3000$ m s^{-1}. It is seen that the maximum values of $\Theta_0(\xi_c, \tau_\ell)$ and $\Phi_0(\xi_c, \tau_\ell)$ exhibit a runaway behaviour as the streamwise coordinate τ_ℓ is increased. Using the ignition value $\tau_{\ell,ig}$ and (3.31) and (3.9), we can determine the ignition distance.

4. The high temperature regime

In the high-temperature regime ($T_c > T^*$), steady-state approximations for OH and O yield a three-step reduced mechanism (Lee & Law 1994) :

$$3H_2 + O_2 \rightarrow 2H_2O + 2H, \tag{I'}$$

$$H + O_2 + M \rightarrow HO_2 + M, \tag{II'}$$

$$H_2 + O_2 \rightarrow HO_2 + H, \tag{III'}$$

where $\omega_{I'} = \omega_{1f}$, $\omega_{II'} = \omega_{9f}$ and $\omega_{III'} = \omega_{10b}$. Here the global steps I', II', and III' respectively represent the effects of the branching ($1f$), termination ($9f$), and initiation ($10b$) reactions. Step III' is relatively slow and is needed only to initiate the radical pool, therefore its contribution to the heat equation is neglected. Furthermore, since the rates of these reactions are not dependent on the concentration of HO_2, only the conservation equations for energy and H are needed to determine the ignition distance in the high-temperature regime.

Owing to the non-unity value of Le_{H}, it is convenient to work in terms of the original coordinate η. We define a new streamwise coordinate

$$\zeta_h = x\left(\frac{2\hat{\rho}\hat{Y}_{\mathrm{H_2},-\infty}}{\hat{u}_\infty W_{\mathrm{H_2}}}\right) A_{1f}\mathrm{e}^{T_{a,1}/T_c}(2-\kappa_c)Y_{\mathrm{O_2},c}, \tag{4.40}$$

which is based on the branching rate of the H radical and where the subscript h designates the high-temperature regime. The factor $(2-\kappa_c)$ captures the dependence of the characteristic length in the high-temperature regime on the termination rate: as the termination rate approaches the branching rate, the distance required for a significant increase in the H concentration increases. The governing equations then become

$$\frac{\partial^2 T}{\partial\eta^2} + f\frac{\partial T}{\partial\eta} - 2\zeta_h f'\frac{\partial T}{\partial\zeta_h} = -\zeta_h k_{1f}\frac{(q_{I'}+q_{II'}\kappa)}{2-\kappa_c}\frac{Y_{\mathrm{O_2}}}{Y_{\mathrm{O_2},c}}Y_{\mathrm{H}} - 2\mu\left[\frac{f''(\eta)}{1-\lambda}\right]^2, \tag{4.41}$$

$$\frac{1}{Le_{\mathrm{H}}}\frac{\partial^2 Y_{\mathrm{H}}}{\partial\eta^2} + f\frac{\partial Y_{\mathrm{H}}}{\partial\eta} - 2\zeta_h f'\frac{\partial Y_{\mathrm{H}}}{\partial\zeta_h} = -\zeta_h\frac{Y_{\mathrm{O_2}}}{Y_{\mathrm{O_2},c}}\left[k_{1f}\frac{2-\kappa}{2-\kappa_c}Y_{\mathrm{H}} + \frac{k_{10b}Y_{\mathrm{H_2}}}{2-\kappa_c}\right], \tag{4.42}$$

where the rate constant k_m is normalized by $\hat{k}_{1f}$ evaluated at T_c. These equations are subject to the boundary conditions shown in (2.5). In (4.41), the reaction term denotes heat generation by the branching $(1f)$ and termination $(9f)$ steps, while the reaction terms of (4.42) consist of radical production and depletion by branching and termination respectively, plus a small initiation that triggers reaction in the initially frozen state. Similar to §3, the analysis for the high-temperature regime is also divided into two situations depending on the parameter α, as presented in the following.

4.1. *The hot-stream case:* $\alpha > 0$

In this regime, the large diffusivity of the H radical significantly affects its concentration profile such that the usual activation energy expansions, as in §3, provide little simplification. To analyse this system properly, we exploit the small-Le_{H} limit as in the study of Sánchez, Liñán & Williams (1994). Defining a new coordinate $\eta_H = Le_{\mathrm{H}}^{1/2}\eta$, and expanding the temperature as $T = T_f + \epsilon_h\phi$, where $\epsilon_h = T_\infty^2/T_{a,1}$, (4.41) and (4.42) become

$$\frac{\partial^2 Y_{\mathrm{H}}}{\partial\eta_{\mathrm{H}}^2} + (Le_{\mathrm{H}}^{1/2}f)\frac{\partial Y_{\mathrm{H}}}{\partial\eta_{\mathrm{H}}} - 2\zeta_h f'\frac{\partial Y_{\mathrm{H}}}{\partial\zeta_h} = -\zeta_h\frac{Y_{\mathrm{O_2}}}{Y_{\mathrm{O_2},\infty}}\left[k_{1f}(T_f)\frac{2\mathrm{e}^{\phi}-\kappa(T_f)}{2-\kappa_\infty}Y_{\mathrm{H}} + \frac{k_{10b}(T_f)Y_{\mathrm{H_2}}}{2-\kappa_\infty}\mathrm{e}^{\gamma\phi}\right], \tag{4.43}$$

$$Le_{\mathrm{H}}\frac{\partial^2\phi}{\partial\eta_{\mathrm{H}}^2} + (Le_{\mathrm{H}}^{1/2}f)\frac{\partial\phi}{\partial\eta_{\mathrm{H}}} - 2\zeta_h f'\frac{\partial\phi}{\partial\zeta_h} = -\zeta_h\frac{Y_{\mathrm{O_2}}}{Y_{\mathrm{O_2},\infty}}k_{1f}(T_f)\frac{q_{I'}\mathrm{e}^{\phi}+q_{II'}\kappa(T_f)}{2-\kappa_\infty}Y_{\mathrm{H}}/\epsilon_h, \tag{4.44}$$

where $\gamma = T_{a,10b}/T_{a,1f}$. The rate constant $k_{1f}(T_f)$ in the preceding equations exponentially decays when $T_\infty - T_f$ becomes $O(\epsilon_h)$. Because the activation energy is large, this occurs at a moderately large value of η. In an activation energy analysis, we would exploit this fact to simplify the governing equations as in §3.1. In this case, however, using the physical values of Le_{H} and $T_{a,1}$ we find that the decay occurs for $\eta_{\mathrm{H}} < 1$ making this type of simplification inappropriate and motivating the small-Lewis-number expansion.

Examining equations (4.43) and (4.44) reveals that once the rise in temperature becomes significant, i.e. $\phi \sim O(1)$, thermal runaway occurs owing to the nonlinear Arrhenius behaviour. When this occurs, a scaling argument reveals that Y_{H} is of $O\left(\epsilon_h(2-\kappa)/(q_{I'}+\kappa q_{II'})\right)$. Anticipating that the distance required for Y_{H} to reach

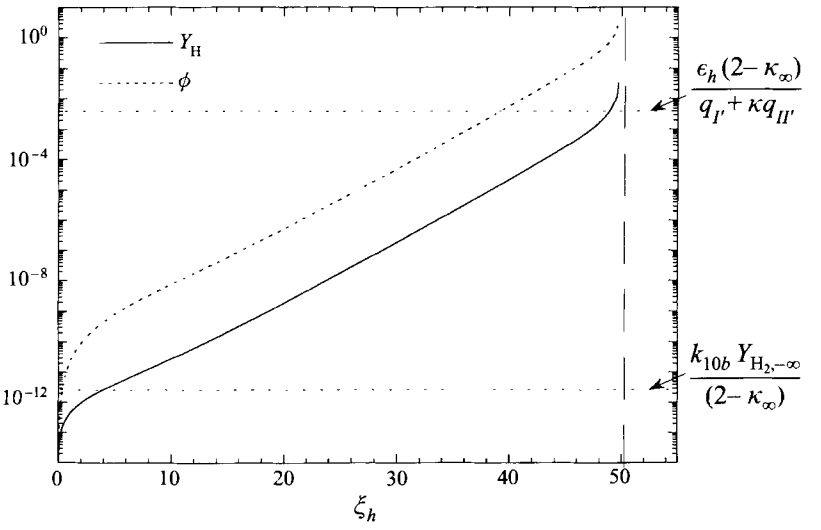

FIGURE 4. Typical behaviour of the solutions to equations (4.43), (4.44) and (2.5) for $\hat{T}_\infty = 1100$ K, $\hat{u}_\infty = 600$ m s^{-1}, and $p = 1$ atm: the maximum values of the perturbed solutions as a function of the non-dimensional streamwise coordinate.

this value is much larger than the distance required for the Arrhenius runaway, we let $\phi \ll 1$ and focus on the Y_H build-up. This decouples equation (4.43) from equation (4.44), allowing an analytic solution of equation (4.43) to be sought. For the ignition criterion, instead of using the location of the thermal runaway, we use the condition

$$Y_H = O\left(\epsilon_h \frac{2-\kappa_\infty}{q_{I'}+\kappa_\infty q_{II'}}\right) \tag{4.45}$$

which causes only small errors relative to the H build-up distance. The reason for these approximations are clarified by figure 4 which is a numerical solution to equations (4.43) and (4.44) calculated in a manner similar to §3.2. It is seen that the distance required for the Y_H build-up is much larger than the distance over which the Arrhenius runaway occurs, and the expression given by (4.43) does capture the approximate location of the Arrhenius runaway. Thus the above approximations are justifiable, and we continue the analysis by examining only equation (4.43).

For $Le_H \ll 1$, several simplifications can be made to (4.43). In terms of the η_H coordinate, the temperature, momentum, and species profiles except for H and H_2, appear as step functions across a thin layer of $O(Le_H^{1/2})$ around $\eta_H = 0$. In this asymptotic limit, we further simplify (4.43) using the relation

$$k_{1f}(2-\kappa)Y_{O_2}(\eta_H) \sim (2-\kappa_\infty)Y_{O_2,\infty}f', \tag{4.46}$$

which allows us to seek an analytic solution to the homogeneous problem for Y_H, i.e. neglecting the initiation term in equation (4.43). Using separation of variables, we obtain

$$Y_H = e^{\zeta_h/2}\sum_{n=0}^{\infty} a_n \zeta_h^{-n-1/2} \begin{cases} U(-1/2-2n, \eta_H)e^{-\eta_H^2/4}, & \eta_H > 0 \\ U(-1/2-2n, \lambda^{1/2}\eta_H)e^{-\lambda\eta_H^{2/4}}, & \eta_H < 0, \end{cases} \tag{4.47}$$

where U is the parabolic cylinder function (Abramowitz & Stegun 1965).

It is noted that the asymptotic relation (4.46) is correct to all orders of Le_H for $\eta_H > O(Le_H^{1/2})$, and is correct to the first two orders in $Le_H^{1/2}$ in the transition zone, therefore the leading-order solution is unaffected in these zones. For $\eta_H < -O(Le_H^{1/2})$, however, the left-hand side of (4.46) is exponentially small while the right-hand side allows reaction to occur at λ times the rate of reaction in the hot stream. Because $\lambda < 1$, this only causes a small difference in the behaviour of the separable solution (4.47) as compared to a numerical solution of (4.43) even for λ as large as 0.5.

The separable solution captures the exponential growth of the H concentration with ζ_h caused by the branching reaction. However, without considering the initiation reaction, there would be no H radicals to trigger this exponential growth, and the result would simply be the trivial solution. To determine the influence of the initiation reaction, we expand the solution for small ζ_h in the form

$$Y_H = \zeta_h N_1(\eta_H) + \zeta_h^2 N_2(\eta_H) + O(\zeta_h^3). \tag{4.48}$$

Substituting this expansion into (4.43) reveals that, for small ζ_h, the branching reaction is negligible owing to the small H concentration such that we obtain a linear streamwise growth of the following form:

$$Y_H \sim \frac{k_{10b} Y_{H_2,-\infty}}{2-\kappa} \zeta_h. \tag{4.49}$$

This linear growth continues until the rates of the branching reaction and the initiation reaction are of equal order, which occurs when

$$Y_H = O\left(\frac{k_{10b} Y_{H_2,-\infty}}{2-\kappa_\infty}\right) \quad \text{at } \zeta_h = 1. \tag{4.50}$$

Again examining figure 4, we see that for small ζ_h, there is indeed a linear growth region which transitions to the behaviour shown by the separable solution, equation (4.47), at the conditions given above. Thus, these conditions are used as initial conditions for the separable solution which then captures the exponential growth of Y_H up to the ignition point.

To obtain the ignition criterion, the condition (4.45) is applied to the separable solution (4.47). This gives the following implicit expression for the ignition distance:

$$\frac{e^{\zeta_{h,ig}/2}}{\zeta_{h,ig}^{1/2}} = \frac{\epsilon_h(2-\kappa_\infty)}{(q_{I'} + \kappa_\infty q_{II'})} \frac{(2-\kappa_\infty)}{k_{10b} Y_{H_2,-\infty}}. \tag{4.51}$$

We remark that the ignition behaviour is mostly governed by the evolution of Y_H given in (4.47), which shows an exponential growth of many orders throughout the ignition process. Therefore, the $O(1)$ constants involved in the scaling arguments in the initial and final states, i.e. (4.45) and (4.50), cause only a small error in the total ignition distance and thus are dropped out in (4.51). To verify this, we have compared the ignition distance predicted by (4.51) with numerical calculations, and it was found that the two results agree within 20% accuracy over a wide range of pressure and temperature. This confirms that the analysis properly captures the leading behaviour of the ignition process, especially the dominance of the Y_H build-up during the ignition delay.

4.2. *The viscous-heating case:* $\alpha < 0$

In this case, reaction starts to take place around $\xi_c = -\alpha/2\mu$, as in §3.2. The frozen temperature profile expanded in the η-coordinate around η_c becomes

$$T_f = T_c - \mu(\xi - \xi_c)^2 = T_c - \mu\left[\frac{f_c''}{1-\lambda}(\eta - \eta_c)\right]^2 + O(\eta - \eta_c)^3. \tag{4.52}$$

Introducing the stretched coordinate

$$Z_h = \left(\frac{\mu}{\epsilon_h}\right)^{1/2} \frac{f_c''}{1-\lambda}(\eta - \eta_c), \tag{4.53}$$

and expanding the inner solutions near $\eta = \eta_c$ as

$$T_{in} = T_c - \epsilon_h Z_h^2 + \epsilon_h(\tilde{\vartheta}_0 + \epsilon_h^{1/2}\tilde{\vartheta}_1) + O(\epsilon_h^2), \tag{4.54}$$

$$Y_{\mathrm{H},in} = \epsilon_h(\tilde{\varphi}_0 + \epsilon_h^{1/2}\tilde{\varphi}_1) + O(\epsilon_h^2), \tag{4.55}$$

we obtain the structure equations at the first two orders as

$$\frac{\partial^2\tilde{\vartheta}_0}{\partial Z_h^2} = 0, \qquad \frac{\partial^2\tilde{\varphi}_0}{\partial Z_h^2} = 0, \tag{4.56}$$

$$\left.\begin{aligned} \frac{\partial^2\tilde{\vartheta}_1}{\partial Z_h^2} &= -\tilde{\Lambda}\frac{\mu^{1/2}f_c''}{1-\lambda}\frac{q_{I'} + q_{II'}\kappa_c}{2-\kappa_c}\tilde{\varphi}_0\exp(\tilde{\vartheta}_0 - Z_h^2), \\ \frac{\partial^2\tilde{\varphi}_1}{\partial Z_h^2} &= -Le_{\mathrm{H}}\tilde{\Lambda}\frac{\mu^{1/2}f_c''}{1-\lambda}\left\{\tilde{\varphi}_0\exp(\tilde{\vartheta}_0 - Z_h^2) + \frac{k_{10b,c}Y_{\mathrm{H_2},c}}{(2-\kappa_c)\epsilon_h}\exp[\gamma_h(\tilde{\vartheta}_0 - Z_h^2)]\right\}, \end{aligned}\right\} \tag{4.57}$$

where

$$\tilde{\Lambda} = \left(\frac{\epsilon_h}{\mu}\right)^{1/2}\frac{(1-\lambda)\zeta_h}{f_c''}. \tag{4.58}$$

The outer solutions are also expanded as

$$T_{out} = T_f(\eta) + \epsilon_h\Xi_0(\eta, \zeta_h) + O(\epsilon_h^{3/2}), \tag{4.59}$$

$$Y_{\mathrm{H},out} = \epsilon_h\Psi_0(\eta, \zeta_h) + O(\epsilon_h^{3/2}), \tag{4.60}$$

such that the leading-order equations for the perturbations in the outer solutions become

$$\frac{\partial^2\Xi_0}{\partial\eta^2} + f\frac{\partial\Xi_0}{\partial\eta} - 2f'\tilde{\Lambda}\frac{\partial\Xi_0}{\partial\tilde{\Lambda}} = -\tilde{\Lambda}q_{II'}\Gamma(T_f)\frac{Y_{\mathrm{O_2}}}{Y_{\mathrm{O_2},c}}\Psi_0, \quad \eta \neq \eta_c, \tag{4.61}$$

$$\frac{1}{Le_{\mathrm{H}}}\frac{\partial^2\Psi_0}{\partial\eta^2} + f\frac{\partial\Psi_0}{\partial\eta} - 2f'\tilde{\Lambda}\frac{\partial\Psi_0}{\partial\tilde{\Lambda}} = \tilde{\Lambda}\Gamma(T_f)\frac{Y_{\mathrm{O_2}}}{Y_{\mathrm{O_2},c}}\Psi_0, \quad \eta \neq \eta_c, \tag{4.62}$$

where

$$\Gamma(T) = k_{1f}\frac{\kappa}{2-\kappa_c}\left(\frac{\mu}{\epsilon_h}\right)^{1/2}\frac{f_c''}{(1-\lambda)} \tag{4.63}$$

with boundary and initial conditions

$$\left.\begin{aligned} &\Xi_0(\infty, \tilde{\Lambda}) = \Xi_0(-\infty, \tilde{\Lambda}) = \Xi_0(\eta, 0) = 0, \\ &\Psi_0(\infty, \tilde{\Lambda}) = \Psi_0(-\infty, \tilde{\Lambda}) = \Psi_0(\eta, 0) = 0. \end{aligned}\right\} \tag{4.64}$$

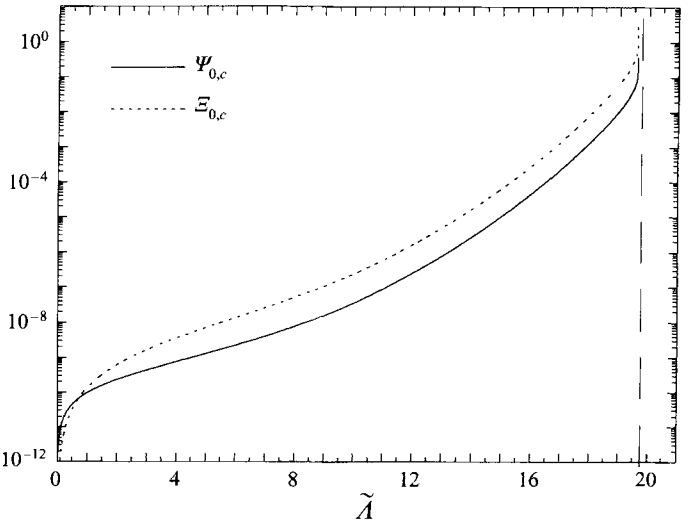

FIGURE 5. Typical behaviour of the solution to equations (4.61)–(4.65) for $\hat{T}_\infty = 1000$ K, $\hat{u}_\infty = 3000$ m s^{-1}, and $p = 1$ atm: the maximum values of the perturbed solutions as a function of the non-dimensional streamwise coordinate.

In deriving these equations, we have assumed that $\kappa_c \leqslant O(\epsilon_h^{1/2})$. This limit is the most interesting because it covers a wide range of ignition conditions while still predicting the correct trends as T_c approaches the crossover temperature, T^*.

Matching the inner- and outer-zone equations reveals that through the inner zone, the temperature perturbation and H mass fraction are essentially constant, but there is an $O(1)$ change in the slope of the outer solution due to the production of heat and radicals in the inner zone. The jump in slope of the outer solution can be obtained by integrating equation (4.57) across the inner zone and matching the inner and outer solutions as

$$\left.\begin{aligned}\left[\frac{\partial \Xi_0}{\partial \eta}\right]_{\eta_c^-}^{\eta_c^+} &= -\pi^{1/2}\tilde{\Lambda}\frac{q_{I'}+q_{II'}\kappa_c}{2-\kappa_c}\Psi_{0,c}e^{\Xi_{0,c}},\\ \left[\frac{\partial \Psi_0}{\partial \eta}\right]_{\eta_c^-}^{\eta_c^+} &= -\pi^{1/2}Le_H\tilde{\Lambda}\left\{\Psi_{0,c}e^{\Xi_{0,c}}+\frac{k_{10b,c}Y_{H_2,c}}{\epsilon_h(2-\kappa_c)\gamma_h^{1/2}}e^{\gamma_h\Xi_{0,c}}\right\}.\end{aligned}\right\} \tag{4.65}$$

We remark that, as in the hot-stream case (§4.1), the distance required for the development of the H radical is large compared to the distance over which the Arrhenius runaway occurs. Thus, we can again use a scaling argument from the temperature evolution equation to determine the ignition distance. However, in this case decoupling the equations for the temperature perturbation and the H mass fraction does not make the analysis amenable to an analytic approach, and thus the coupled system is solved numerically.

Numerical solution for the system (4.61)–(4.65) has been obtained in a manner similar to that described in §3.2 for conditions of 1 atm, $\hat{T}_\infty = 1000$ K, and $\hat{u}_\infty = 3000$ m s^{-1}. In figure 5 we plot the maximum values of the perturbed quantities, $\Xi_0(\eta_c, \tilde{\Lambda})$ and $\Psi_0(\eta_c, \tilde{\Lambda})$, versus $\tilde{\Lambda}$. Similar to the hot-stream case, we can identify an initiation and a branching regime characterized by linear and exponential growth respectively. In addition, these values exhibit a runaway behaviour at $\tilde{\Lambda}_{ig}$ where the

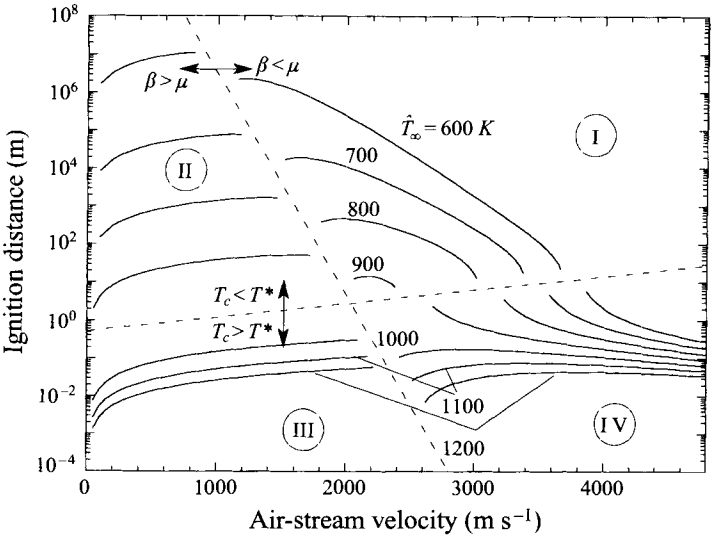

FIGURE 6. Ignition distance as a function of the hot-stream velocity for various $\hat{T}_\infty$ at $p = 1$ atm.

temperature perturbation, Ξ_0, becomes $O(1)$. Knowing the ignition value $\tilde{A}_{ig}$ and using (4.58) and (4.40), we obtain the ignition distance.

5. Results and discussion

The analysis of the four different regimes in §3 and §4 covers the entire range of parameters. To determine which analysis is applicable to given conditions of the system, we must evaluate two quantities in advance, namely $T_c - T^*$ and α. In the following, we vary the parameters $\hat{u}_\infty$, $\hat{T}_\infty$ and p, and plot the results appropriate to those conditions.

Figures 6 and 7 respectively show the ignition distance as a function of the air-stream velocity and Mach number, for various air-stream temperatures. The plot of figure 6 provides a direct indication of the extent of viscous heating for various $\hat{T}_\infty$, while the plot of figure 7, in terms of M_∞, is a more conventional aerodynamical representation. In each figure we have inserted two dotted lines to distinguish the four different cases of analysis. For example, quadrant I is the viscous-heating case in the low-temperature regime ($\beta < \mu$, $T_c < T^*$), etc. Furthermore, while the solutions are discontinuous between neighbouring regimes because a different analysis is conducted, the trend exhibited by the individual curves in approaching the respective transition boundaries is real. For example, for the low-temperature regimes, the decreasing trend of the ignition distance as the transition boundary is approached for both the hot-stream and viscous-heating cases indicates the attainment of a maximum ignition distance as the dominant ignition source changes its characteristics. A separate analysis for the intermediate situation that is valid for $\alpha = O(\epsilon^{1/2})$ (Im *et al.* 1994) can be performed to provide smooth transitions. Similarly, the transition behaviour between the low- and high-temperature regimes can be described by an additional asymptotic analysis around the second-explosion limit represented by

$$2\omega_{1f} = \omega_{9f} \quad \rightarrow \quad 2\hat{k}_{1f} = \hat{k}_{9f}[\mathrm{M}], \tag{5.1}$$

which is a simple balance between the dominant branching and termination reactions

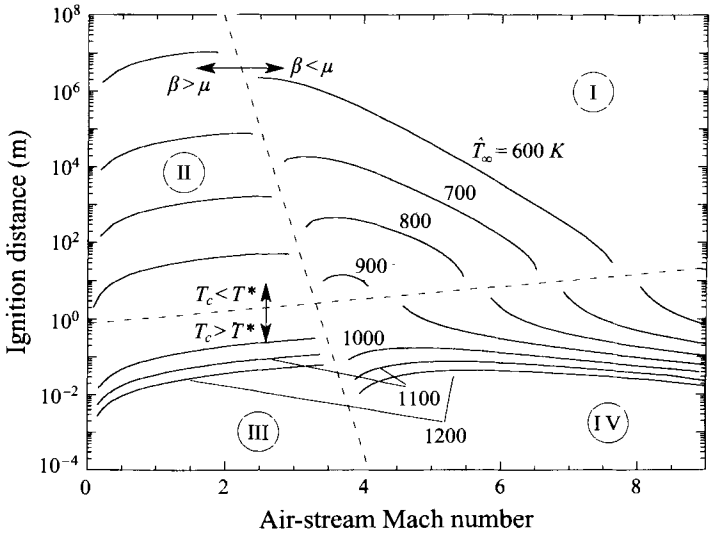

FIGURE 7. Ignition distance as a function of the hot-stream Mach number for various $\hat{T}_\infty$ at $p = 1$ atm.

obtained by making steady-state approximations for H, OH and O (Lee & Law 1994). These transition analyses are not presented because the present results adequately exhibit the global behaviour of the ignition response.

Figures 6 and 7 thus show that, as the velocity is increased in the subsonic limit, the viscous heating effect is not significant so that the ignition distance increases linearly with velocity as the reactant is swept further downstream for higher local streamwise velocity. As the velocity increases further, viscous heating, which is proportional to $\hat{u}_\infty^2$, becomes effective such that the ignition distance passes through a maximum value and then decreases. This gross trend is similar to that of the one-step chemistry analysis (Im *et al.* 1993, 1994).

The use of the more realistic hydrogen oxidation chemistry in the present analysis, however, has captured several distinguishing features of the ignition response. First, the ignition distance exhibits different sensitivity to the maximum frozen temperature, T_c, which varies either by a direct change in T_∞ or by an increase in viscous heating through a velocity increase. As shown in §3 and §4, the low-temperature regime is mainly controlled by the branching of H_2O_2 (step $15f$), while the high-temperature regime depends strongly on the chain branching step $1f$. Since $E_{a,15f}$ is much larger than $E_{a,1f}$, it is expected that the ignition distance is more temperature sensitive in the low-temperature regime, i.e. $T_c < T^*$, where $\hat{T}^* = 925\,\mathrm{K}$ at 1 atm. In the hot-stream case (quadrants II and III) the difference in the sensitivity is reflected by the larger slope in the low-temperature regime. This is because for hot-stream ignition we expect $x_{ig} \sim \hat{u}_\infty \exp(E_a/R^0\hat{T}_\infty)$, where E_a is the controlling activation energy. Since the low-temperature regime not only has a smaller $\hat{T}_\infty$ but also a larger E_a, the Arrhenius factor, $\exp(E_a/R^0\hat{T}_\infty)$, is correspondingly larger. This implies that x_{ig} as well as its rate of increase with $\hat{u}_\infty$ are both larger.

For the viscous heating case, the difference in sensitivity between the low- and high-temperature regimes is even more prominent in that, while x_{ig} decreases rapidly with $\hat{u}_\infty$ in the low-temperature regime, the decrease is substantially gentler for the high-temperature regime. Here $x_{ig} \sim \hat{u}_\infty \exp(E_a/R^0\hat{T}_c)$, where $\hat{T}_c \sim M_\infty^2$. Thus for high-$M_\infty$

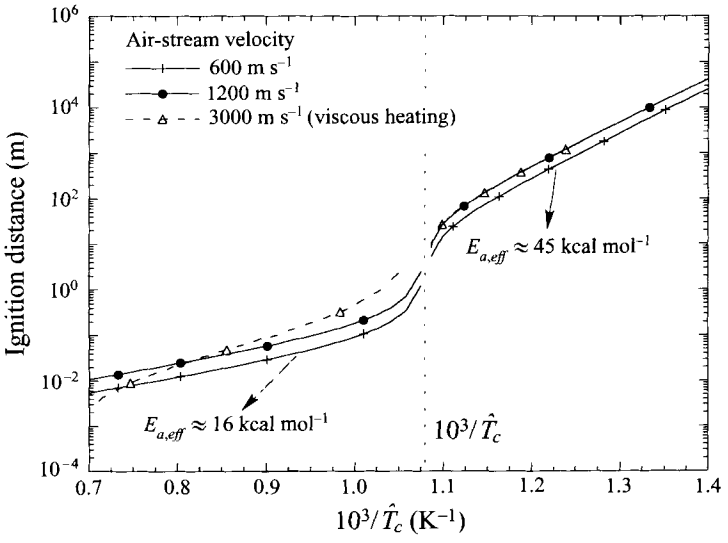

FIGURE 8. Ignition distance as a function of the reciprocal of the maximum frozen temperature for various $\hat{u}_\infty$ at $p = 1$ atm.

flows, the influence of $\hat{u}_\infty$ through the Arrhenius factor dominates. Consequently, a smaller E_a for the high-temperature regime implies a greatly reduced sensitivity of x_{ig} with $\hat{u}_\infty$. The above results therefore demonstrate that viscous heating is more effective in enhancing ignition when the characteristic temperature of the system is lower than the crossover temperature. From the practical point of view, however, it is unfortunate that the largest decrease in the ignition distance occurs in the relatively low-temperature system where the ignition distances are impractically large unless the flow speed is extremely large, while in the high-temperature regime the ignition enhancement by viscous heating appears to be less significant owing to the smaller temperature sensitivity of the key reaction step.

The characteristic of the temperature sensitivity is shown more clearly in figure 8, in which the variation of the ignition distance is plotted as a function of the reciprocal of the maximum characteristic temperature, $\hat{T}_c$, for various hot-stream velocities. Note that, for a given $\hat{u}_\infty$, $\hat{T}_c$ increases with increasing $\hat{T}_\infty$. Here the solid and dotted curves respectively denote the hot-stream and the viscous-heating cases; the viscous-heating curve for $\hat{u}_\infty = 3000$ m s^{-1} breaks down around $10^3/\hat{T}_c \approx 0.8$ because the analysis loses its accuracy as $\hat{T}_c$ increases to reduce the parameter α. It is seen that, for both the hot-stream and viscous-heating cases, the general temperature sensitivity is determined by whether the maximum frozen temperature falls into the high- or the low-temperature regime. Thus in the Arrhenius plot of figure 8, the slope of the curve readily yields a system activation energy. These values are found to be approximately 45 and 16 kcal mole^{-1} for the low- and high-temperature regimes respectively, which are very close to $E_{a,15f}$ and $E_{a,1f}$ shown in table 1. It is of interest to note that a similar result was reported (Skinner & Ringrose 1965) for the ignition delay of homogeneous hydrogen/oxygen mixtures measured in a shock tube. What is significant in the present result is that the same chemical behaviour is manifested for a diffusive, non-premixed system. This result, on the other hand, is not surprising by recognizing that $x_{ig} \sim \exp(E_a/R^0\hat{T}_c)$, where E_a is representative of a dominant chain branching reaction in a kinetic mechanism.

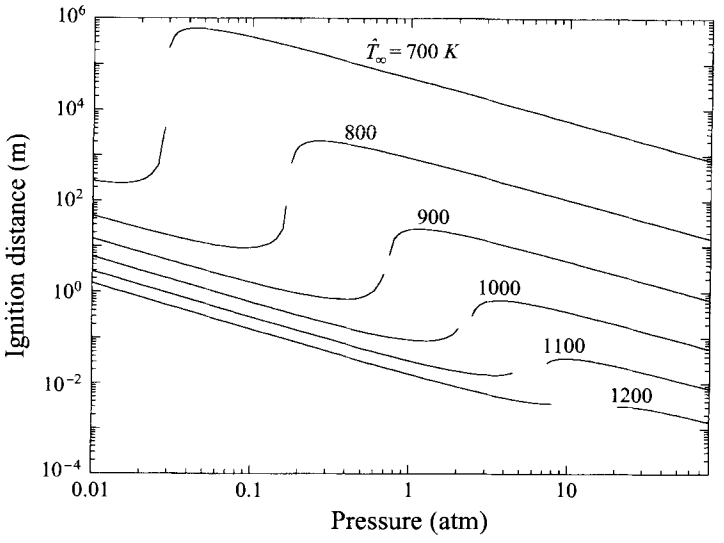

FIGURE 9. Ignition distance as a function of pressure for various $\hat{T}_\infty$ in the hot-stream case, $\hat{u}_\infty = 600$ m s^{-1}.

Another parameter of interest which can sensitively affect the reaction rates is the system pressure. The influence of pressure on the net reaction rate of a complex reaction scheme can be quite subtle in that, while increasing pressure generally increases the rate of an elementary reaction, the extent of influence depends on the molecularity of the reaction. For example, the reaction rate varies with p^2 and p^3 for two- and three-body reactions respectively. Since three-body reactions are generally terminating and hence have a net retarding effect on the overall reaction rate, while two-body reactions are mostly branching and hence tend to promote the net reaction rate, there exist situations in which an increase in the system pressure could actually lead to a reduction in the net reaction rate (Egolfopoulos & Law 1990).

Figures 9 and 10 plot the ignition distance as a function of pressure, for various hot-stream temperatures. In each figure the hot-stream speed is fixed in order to maintain the same amount of viscous heating, such that figures 9 and 10 respectively show the hot-stream case ($\hat{u}_\infty = 600$ m s^{-1}) and the viscous-heating case ($\hat{u}_\infty = 3000$ m s^{-1}). Both figures clearly demonstrate the 'Z-curve' behaviour (Lewis & von Elbe 1987) that has been found in the homogeneous explosion problem. That is, the high- and low-temperature solutions respectively correspond to the first and third limits in the homogeneous system, as demonstrated by Lee & Law (1994). Each curve shows the transition from the high-temperature regime to the low-temperature regime as the pressure is increased to a *crossover pressure*, at which the reaction rates of the branching and termination steps are equal. Different temperature sensitivity is also shown here: as the hot-stream temperature is increased by the same amount, the curves drop more significantly for the high-pressure and the low-temperature regimes, so that the relatively large jump in the ignition distance through the transition to the low-temperature chemistry is not observed at higher $\hat{T}_\infty$.

The non-monotonic response of the curves in figures 9 and 10 can be explained on the basis of the hydrogen/oxygen homogeneous explosion limits (Lewis & von Elbe 1987) by considering the ignitability of a flow for a given ignition distance, x_{ig}. Thus by fixing x_{ig}, say at 1 m, it is seen that with increasing pressure the system

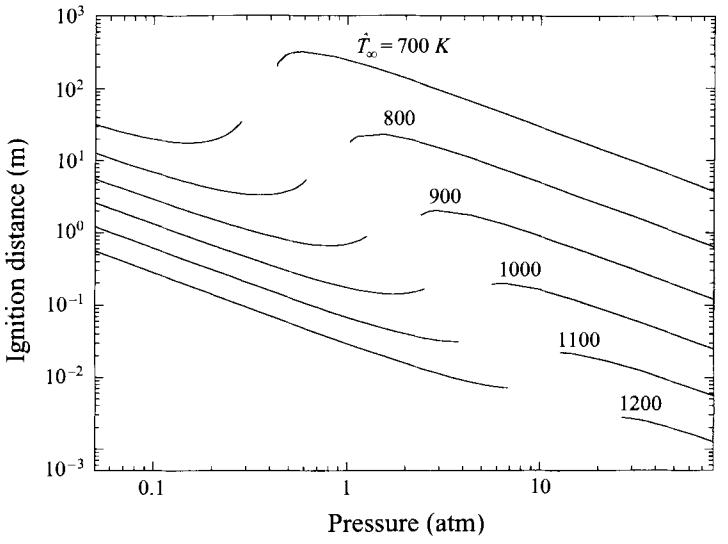

FIGURE 10. Ignition distance as a function of pressure for various $\hat{T}_\infty$ in the viscous-heating case, $\hat{u}_\infty = 3000$ m s^{-1}.

changes from one of non-ignition, to ignition, to non-ignition, and finally to ignition again. In the low-pressure regimes, the difficulty in achieving ignition is due to the significant loss from the reaction region as compared to the reduced reactivity of the branching reaction $1f$ because of the low pressure. With increasing pressure, reaction $1f$ is facilitated and hence leads to ignition. A further increase in pressure, however, promotes the three-body termination reaction $9f$ relative to the two-body branching reaction $1f$, and eventually suppresses ignition. Finally, at very high pressures, the abundance of H_2O_2 activates the branching reaction $15f$, and consequently renders the system ignitable again.

It is noted that the turning of the ignition distance curve in the high-temperature regime is due to depletion of the H radical through the termination reaction, which is properly captured by the present high-temperature reduced mechanism. However, if we adopt the mechanism of Treviño & Méndez (1991), which assumes steady state of HO_2, the result shows that the ignition distance curve monotonically decreases as pressure increases until the crossover value is reached. These two mechanisms merge when the characteristic temperature is sufficiently high. Therefore, it can be concluded that, although the two-step mechanism of Treviño & Méndez (1991) yields the correct trend for sufficiently high temperatures, the present mechanism, which is basically two-step, is preferred because it captures the intermediate behaviour when the temperature approaches the crossover value, with no additional complication in the analysis.

We further observe in figures 9 and 10 that, except near the crossover pressure, the ignition distance decreases almost linearly with a slope which is approximately -1 in the logarithmic plot. Recognizing that the reaction terms in the original energy and species equations (2.3) and (2.4) are divided by $\hat{u}_\infty\hat{\rho}$ and since $\hat{u}_\infty$ is fixed here, the behaviour of $x_{ig} \sim p^{-1}$ implies that the reaction order is two. This is not surprising because ignition in these pressure ranges is governed by the second-order branching steps $1f$ and $15f$ for low and high pressures respectively. When pressure is close to the crossover value ($\kappa \to 2$), however, other competing effects become important in

characterizing ignition, such that a simple second-order behaviour no longer holds. In fact, the positive slope of the curves near the crossover pressure implies that the overall reaction order becomes less than one and possibly even negative, as discussed in Egolfopoulos & Law (1990).

We finally comment that several assumptions have been made in the present study in order to simplify the problem for an analytic approach. Some of those assumptions, however, may lead to significant errors in the quantitative prediction of ignition distances. In particular, the constant Chapman–Rubesin parameter ($\hat{\rho}\hat{\mu}$) can be a poor assumption in the present hydrogen/air system in which the density varies widely within the mixing layer (Nishioka & Law 1995). That is, evaluating $\hat{\rho}\hat{\mu}$ based on the air stream may lead to a significant overestimation of $\hat{\mu}$ throughout the mixing layer, which may in turn result in a considerable underestimation of the ignition distance, especially when viscous heating is the dominant source of ignition. A careful choice of property values is therefore necessary when comparing the present result with quantitative data.

6. Conclusions

We have performed an analysis of ignition within the supersonic hydrogen/air mixing layer, using activation energy asymptotics with reduced chemistry. Two distinct reduced mechanisms have been adopted depending on the characteristic temperature of the reaction zone relative to the crossover temperature. In contrast to a previous study (Treviño & Méndez 1991), we have used a two-step mechanism for the low-temperature regime and an effectively two-step mechanism for the high-temperature regime, which have been shown to be more appropriate to describe the ignition behaviour for a wider range of parameters. Analysis of each regime has been further divided into two cases, namely the hot-stream and the viscous-heating cases, depending on the relative dominance of the ignition energy source. In the low-temperature regime, consistent with the previous thermal ignition studies with single-step chemistry (Im *et al.* 1993, 1994), the reaction zone structure was found to be locally similar in the hot-stream case, so that ignition is identified by the existence of the turning point behaviour. Whereas in the viscous-heating case, the effect of flow non-similarity becomes important, and the solution shows the thermal runaway behaviour at ignition, also consistent with the one-step chemistry analysis. The behaviour in the high-temperature regime, however, differs quite substantially from that of the one-step analysis. Owing to the large diffusivity of the H radical, both the hot-stream and viscous-heating cases retain their evolutionary nature. This necessitates the consideration of the initiation step in the early stage of the ignition process which then leads to branching of the H radical through reaction $1f$. The branching process dominates the ignition delay, increasing Y_H by many orders of magnitude and eventually giving off enough heat for ignition through an Arrhenius runaway of the reaction rates.

Predicted ignition distances have been mapped out over the entire range of parameters. First, the present result confirms the existence of a maximum in the ignition distance as the free-stream velocity increases, consistent with the previous analysis with one-step chemistry (Im *et al.* 1994). Furthermore, consideration of the realistic hydrogen/air chemistry yields a rich spectrum of responses. For example, the activation energy of the characteristic branching step in the low-temperature-chemistry regime is much larger than that in the high-temperature chemistry-regime, and therefore the ignition distance is found to be more sensitive to the variation of the characteristic temperature.

When the ignition distance is plotted as a function of pressure, we have demonstrated the non-monotonic response of the ignition distance with increasing pressure. This unique behaviour can be explained on the basis of the homogeneous explosion limits, and distinguishes the ignition dynamics of the hydrogen/oxygen system from that of the previous one-step model problem (Im *et al.* 1994).

Solutions for the four regimes of analysis were shown to match reasonably well with each other, thereby providing a global picture of the ignitibility of the hydrogen/air mixture in the supersonic boundary layer in all possible parameter space.

This research was supported by the Army Research Office under Grant No. DAAL03-GO-0220 and the Air Force Office of Scientific Research under Grant Nos. F49620-92-J-0227 and F49620-93-I-0427. B.T.H. was also partially supported by an Upton graduate fellowship and S.R.L. by the Korea Science and Engineering Foundation. The authors appreciate stimulating discussions with Drs J. K. Bechtold and T. G. Kreutz of Princeton University during this study.

REFERENCES

ABRAMOWITZ, M. & STEGUN, A. 1965 *Handbook of Mathematical Functions*, pp. 686–697.

EGOLFOPOULOS, F. N. & LAW, C. K. 1990 Chain mechanisms in the overall reaction orders in laminar flame propagation. *Combust. Flame* **80**, 7.

FIGUEIRA DA SILVA, L. F., DESHAIES, B., CHAMPION, M. & RENE-CORAIL, M. 1993 Some specific aspects of combustion in supersonic H_2-air laminar mixing layers. *Combust. Sci. Tech.* **89**, 317.

GROSCH, C. E. & JACKSON, T. L. 1991 Ignition and structure of a laminar diffusion flame in a compressible mixing layer with finite rate chemistry. *Phys. Fluids* A **3**, 3087.

IM, H. G., BECHTOLD, J. K. & LAW, C. K. 1993 Analysis of thermal ignition in supersonic flat-plate boundary layers. *J. Fluid Mech.* **249**, 99.

IM, H. G., CHAO, B. H., BECHTOLD, J. K. & LAW, C. K. 1994 Analysis of thermal ignition in the supersonic mixing layer. *AIAA J.* **32**, 341.

JACKSON, T. L. & HUSSAINI, M. Y. 1988 An asymptotic analysis of supersonic reacting mixing layers. *Combust. Sci. Tech.* **57**, 129.

KLEMP, J. B. & ACRIVOS, A. 1972 A note on the laminar mixing of two uniform parallel semi-infinite streams. *J. Fluid Mech.* **55**, 25.

KREUTZ, T. G. & LAW C. K. 1996 Ignition in nonpremixed counterflowing hydrogen versus heated air: computational study with detailed chemistry. *Combustion Flame* **104**, 157.

LEE, S. R. & LAW, C. K. 1994 Asymptotic analysis of ignition in nonpremixed counterflowing hydrogen versus heated air. *Combust. Sci. Tech.* **97**, 377.

LEWIS, B. & ELBE, G. VON 1987 *Combustion, Flames and Explosions of Gases*, 3rd edn. Academic.

LOCK, R. C. 1951 The velocity distribution in the laminar boundary layer between parallel streams. *Q. J. Mech. Appl. Maths* **4**, 42.

MARBLE, F. E. & ADAMSON, T. C. 1954 Ignition and combustion in a laminar mixing zone. *Jet Propulsion* **24**, 85.

NISHIOKA, M. & LAW C. K. 1995 A numerical study of ignition in the supersonic hydrogen/air laminar mixing layer. *AIAA Paper* 95–0377.

SÁNCHEZ, A. L., LIÑÁN, A. & WILLIAMS, F. A. 1994 A bifurcation analysis of high temperature hydrogen oxygen ignition *Twenty-Fifth Symp. (Intl) on Combustion*, pp. 1529–1537. The Combustion Institute, Pittsburgh.

SKINNER, G. B. & RINGROSE, G. H. 1965 Ignition delays of a hydrogen-oxygen-argon mixture at relatively low temperatures. *J. Chem. Phys.* **42**, 2190.

TREVIÑO, C. 1991 Ignition phenomena in H_2-O_2 mixtures. In *Dynamics of Deflagrations and Reactive Systems: Flames.* (ed. A. L. Kuhl, J. C. Leyer, A. A. Borisov & W. A. Sirignano). Progress in Astronautics and Aeronautics, vol. 131, pp. 19–43. AIAA.

TREVIÑO, C. & MÉNDEZ, F. 1991 Asymptotic analysis of the ignition of hydrogen by a hot plate in a boundary layer flow. *Combust. Sci. Tech.* **78**, 197.